Angle-resolved inverse-photoemission study of the nearly perfect TiO_2(110) surface

A. K. See, M. Thayer,* and R. A. Bartynski
Department of Physics and Astronomy and Laboratory for Surface Modification, Rutgers—The State University of New Jersey, Piscataway, New Jersey 08855-0849
(Received 2 September 1992)

We present angle-resolved inverse-photoemission (IPE) spectroscopy data from the nearly perfect TiO_2(110) surface. Results from two high-symmetry directions of the surface Brillouin zone, $\bar{\Gamma}$-$\bar{X}$ and $\bar{\Gamma}$-$\bar{X}'$, are reported and compared with the results of bulk and surface electronic-structure calculations. Features in the spectra appearing ~1, 4, 9, and 13 eV above the Fermi level are associated with the primarily Ti-derived $2t_{2g}$, $3e_g$, $3a_{1g}$, and $4t_{1u}$ levels. The results are consistent with earlier studies using x-ray-absorption spectroscopy and electron-energy-loss spectroscopy but show some discrepancies in energy positions. All of the spectral features exhibit a small amount of dispersion with respect to $k_{\parallel}$. Surface states and resonances identified in the 0–2-eV region are in accordance with previously published calculations [S. Munnix and M. Schmeits, Phys. Rev. B **30**, 2202 (1984)]. The absence of surface resonances near 3 eV strongly suggests that the nearly perfect TiO_2(110) surface is terminated by a bridging oxygen layer.

I. INTRODUCTION

In recent years, the electronic properties of transition-metal-oxide surfaces have received considerable attention.[1] Among them, the surfaces of rutile TiO_2 have generated a great deal of interest due to their important role as supports for metal catalysts. In particular, TiO_2(110) has become a prototype oxide surface, since a nearly perfect surface is relatively easy to prepare and the density of surface defects can be readily changed and controlled. The occupied electronic states of TiO_2(110) have been studied with a number of techniques.[1] Ultraviolet photoelectron spectroscopy (UPS), in particular, has played an important role in probing the valence band of this system.[2–8] For the nearly perfect surface, the valence band is characterized by a broad emission feature centered about 6 eV below E_F. These levels are composed of primarily O $2p$ orbitals that can be further decomposed into bonding (σ) and nonbonding (π) components.[8] On the nearly perfect (110) surface, there are no surface states observed in the ~3-eV-wide bulk band gap, and the Fermi level is pinned just below the bottom of the conduction band by the formation of bulk oxygen vacancies.[4]

In comparison, little is known about the unoccupied electronic states of TiO_2(110). A qualitative picture of the unoccupied levels can be obtained from an empirical symmetry-determined molecular-orbital (MO) scheme and has been used to interpret near-edge features[9–12] with considerable success. A MO energy-level diagram[9] for a $(TiO_6)^{8-}$ cluster is shown in Fig. 1. This diagram applies to all transition-metal oxides in which the metal atom is bound to six oxygen ligands in a site of octahedral symmetry. In the case of the $(TiO_6)^{8-}$ cluster, the π and σ orbitals are completely filled, giving rise to a valence band that is primarily of oxygen $2p$ character, while the $2t_{2g}$ and $3e_g$ orbitals, which are primarily Ti $3d$ derived, are the lowest unoccupied orbitals in the system. Formally, the tetragonal nature of the rutile structure breaks the octahedral symmetry of the cation sites and leads to additional splitting of these levels. Of course, these symmetry considerations will not provide quantitative energy spacings between the levels, and further modification of this picture is expected from solid-state effects.

In previous x-ray-absorption spectroscopy (XAS) and high-energy electron-energy-loss spectroscopy (EELS) studies[9–12] of $3d$ transition metals and their oxides, features related to the $2t_{2g}$, $3e_g$, $3a_{1g}$, and $4t_{1u}$ molecular orbitals have been identified in the near-edge structure

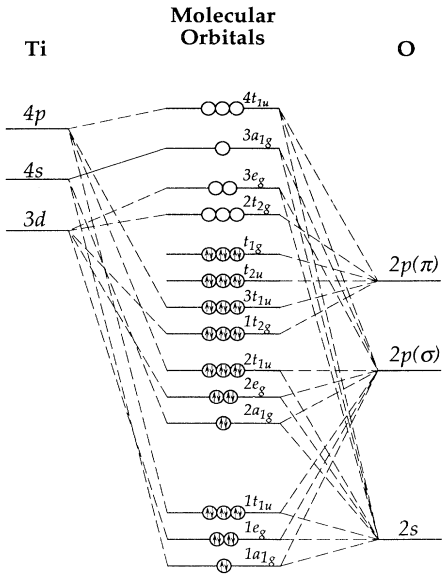

FIG. 1. Schematic MO energy-level diagram (Ref. 10) of a $(TiO_6)^{8-}$ cluster (not drawn to scale).

(NES) of K- and L-shell core excitations. Since the initial states in these excitations are tightly bound core levels, it is generally believed that the NES of these spectroscopies projects out the unoccupied states in the conduction-band local to the site of the core hole. However, the empty levels that are probed in this fashion are subject to modification in energy position due to the presence of a core hole which is poorly screened from the excited electron. Moreover, these techniques are usually not surface sensitive. By using lower excitation energies, the probing depth of EELS can be reduced, and this technique has been used to study the transitions from O $2p$ orbitals to the unoccupied levels.[4,5,13] However, these transitions originate from a broad valence band, and it is therefore difficult to extract much information about the unoccupied states in the conduction band.

Bonding at the $TiO_2(110)$ surface can differ from that in the bulk. The coordination of surface cations may be reduced to 5, or, in some models, even 4. Furthermore, the most easily created surface defects are expected to be oxygen vacancies, which should radically change the electronic properties of the surrounding cations and therefore should have a strong influence on the unoccupied electronic states. In an effort to directly explore these Ti-derived levels, to characterize empty surface electronic states, and to determine how the electronic structure is modified upon defect formation, we have performed angle-resolved inverse photoemission (IPE) studies on both the nearly perfect and the defective $TiO_2(110)$ surfaces. This paper will concentrate on the nature of the nearly perfect surface. Results from the defective surface are published elsewhere.[14]

The rest of this paper is organized as follows. In the next section, some experimental details will be described. The angle-resolved IPE spectra along the two high-symmetry directions of the surface Brillouin zone (SBZ) will be presented and discussed in Sec. III. Finally, we summarize our results in Sec. IV.

II. EXPERIMENTAL CONSIDERATIONS

The data were obtained using an angle-resolved inverse photoemission spectrometer that operates in the isochromat mode. The apparatus is composed of an electron gun and a Geiger-Müller (GM) detector, both of which were fabricated in-house. The electron gun, based on the design of Stoffel and Johnson,[15] produced an electron beam whose angular divergence is less than 4°, resulting in an uncertainty in parallel momentum $\Delta k_{\parallel}$ of $\sim\pm 0.05$ Å^{-1}. The GM detector has a SrF_2 window, is filled with I_2 gas, accepts a solid angle of ~ 0.4 sr and was separated from the electron gun by an angle of 57°. The combination of the ionization threshold of I_2 and the transmittance cutoff of SrF_2 provides a bandpass centered at about 9.5 ± 0.2 eV.[16,17] A previous publication describes this instrumentation in more detail.[18,19] Different incident electron angles were selected by rotating the sample about an axis that was normal to the plane containing the electron gun and the GM detector. At each angle of incidence, the kinetic energy of the incident electrons was typically ramped from 4 to 16 eV and the intensity of 9.5-eV photons was measured. All experiments were performed in an ultrahigh vacuum (UHV) chamber with a base pressure of $\sim 2\times 10^{-10}$ torr. All of the spectra presented in the following section have their energies referenced to the Fermi level (E_F), which was determined by the onset of emission in IPE spectra taken from a tantalum plate in electrical contact with the sample. The chamber was also equipped with low-energy electron-diffraction (LEED) optics and a double-pass cylindrical mirror analyzer (CMA) with a concentric electron gun for Auger electron spectroscopy (AES).

The sample was a commercially produced[20] $TiO_2(110)$ crystal with one side polished. To obtain an atomically clean, well-ordered, and stoichiometric surface, the sample was typically sputtered with 0.5-keV Ar^+ ions (~ 8 μA/cm^2) for about 10 min, and subsequently annealed to about 1000 K for about 1 h. Electron bombardment was used for annealing, and the sample temperature was monitored through a thermocouple mounted on the Ta sample holder. AES showed that the sample was atomically

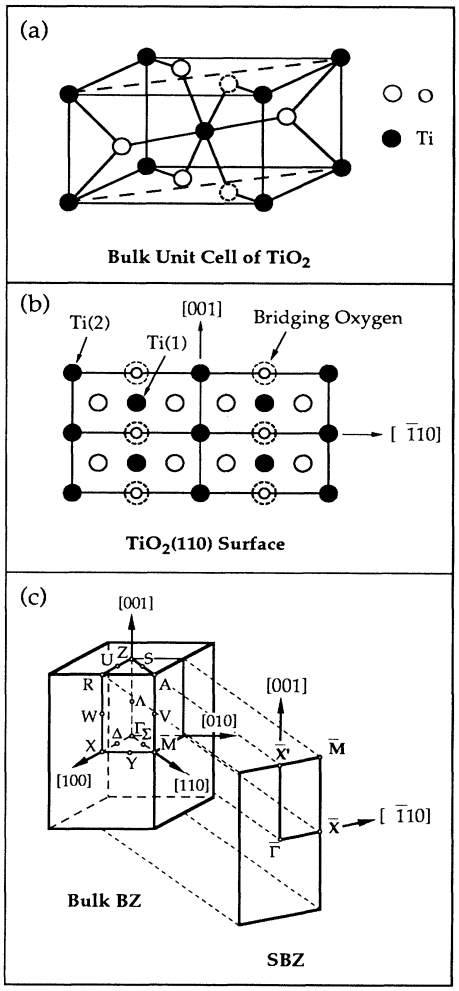

FIG. 2. (a) The bulk unit cell of rutile TiO_2. (b) The unit net of the (110) surface. (c) The bulk Brillouin zone of TiO_2 and the surface Brillouin zone (SBZ) of the (110) surface.

clean after only a few cycles of sputtering and annealing. A sharp LEED pattern and an oxygen (510 eV) to titanium (380 eV) Auger peak height ratio of ~ 1.8, both characteristic of the nearly perfect (110) surface,[5] were observed after this preparation. Previous studies have found[3] that after numerous cycles of sputtering and annealing, the bulk oxygen content of the sample is so depleted that there is insufficient oxygen mobility to restore surface stoichiometry through thermal diffusion from the bulk. In that case, annealing in an oxygen partial pressure after sputtering is needed to achieve the nearly perfect surface stoichiometry. When this experiment was performed, the nearly perfect surface was obtained by annealing the sample in vacuum after sputtering. We have also tested the procedure of annealing the sputtered sample for ~ 1 h in vacuum, followed by several minutes in $\sim 1\times 10^{-6}$-torr oxygen, and subsequently cooling to room temperature in oxygen for a few additional minutes. AES, LEED, and IPE showed no noticeable difference between these two different sample preparation methods.

The bulk unit cell of rutile TiO_2 is shown in Fig. 2(a). Every cation (Ti^{4+}) is surrounded by six anions (O^{2-}), and each anion is bonded to three cations. The (110) surface [Fig. 2(b)], is formed by cutting diagonally across the unit cell along the dashed lines. It is generally believed that the surface is terminated by a layer of oxygen atoms (dashed circles), each bridging two Ti atoms. This model leads to two distinct surface Ti sites: the cations on the four corners of the surface unit cell [Ti(2)] are coordinated to five anions, while the cations at the center of the unit cell [Ti(1)] are sixfold coordinated. When the bridging oxygen layer is removed, the coordination number of Ti(1) changes from 6 to 4, while that of Ti(2) remains unchanged. The bulk Brillouin zone (BZ) of rutile TiO_2 and SBZ of the (110) surface are shown in Fig. 2(c).

III. RESULTS AND DISCUSSION

Typical inverse photoemission spectra from the nearly perfect TiO_2(110) surface obtained at different angles of incidence along the $\bar{\Gamma}$-$\bar{X}$ and $\bar{\Gamma}$-$\bar{X}'$ azimuths are shown in Figs. 3(a) and 3(b), respectively. All spectra in these two azimuths are characterized by two broad features which span from 0 to 2 and 4 to 6 eV above E_F, and whose relative intensities and detailed line shapes change with incident angle. The first broad peak appears to contain at least two components. At some angles of incidence there is evidence of a third feature in this energy region. However, the constituents of this broad peak are never clearly resolved. The high-energy feature located about 4.5 eV above E_F might also contain several overlapping features. Owing to the relatively low signal to background ratio in this energy region, however, we are unable to explore the internal structure of this peak, and only report the observed energy of the local maximum.

Rather than using a visual assignment of peak positions to the structure in the spectra, we have attempted to apply a more systematic approach toward establishing the energies of the unresolved peaks within the low-energy feature. To do this, we subtracted a smooth background composed of a second degree polynomial added to a constant, originating at the Fermi level and extending to ~ 6 eV [cf. Fig. 3(a)]. The true shape of this background, which must account for inelastic scattering and indirect transitions, is not known. The form chosen here is characteristic of the threshold line shape in angle-resolved IPE spectra when no direct transitions are present.[21] Any change in the assigned peak positions resulting from a density-of-states-related structure in this background would be less than the quoted error bars. Once the background was subtracted, the remaining intensity was fitted with three Gaussians, whose peak positions are indicated by the tick marks in Figs. 3(a) and 3(b). When the quality of a two-peak fit was indistinguishable from a three-peak fit, only two features are reported. This procedure yielded peak positions close to those inferred from a visual inspection of the structure in the raw data. In the following discussion, A, B, and C (A', B', and C') refer to these low-energy features along the $\bar{\Gamma}$-$\bar{X}$ ($\bar{\Gamma}$-$\bar{X}'$) azimuth, while D (D') refers to the peak in the high-energy feature. When only two features are evident at low energies, the assignment of the second feature to B or C is clear from the trend indicted by the adjacent spectra, acquired at angular increments of 2.5°.

In the $\bar{\Gamma}$-$\bar{X}$ direction, A is the most pronounced feature in the normal-incidence spectrum, and remains so as the incident angle is increased. Features B and C are consistently weaker and appear to merge or disappear at some incident angles. Feature D exhibits an antibonding dispersion in the sense that its energy decreases with increasing angle of incidence. Along $\bar{\Gamma}$-$\bar{X}'$, feature A' is again dominant at normal incidence, but the intensity of either B' or C' is greater at larger angles. Similar to the other high-symmetry direction, feature D' exhibits a downward dispersion.

In inverse photoemission, as the incident electron enters the sample, the component of its momentum parallel to the surface, $\mathbf{k}_\parallel$, is conserved to within a surface reciprocal-lattice vector $\mathbf{g}_\parallel$. Hence, for $\mathbf{g}_\parallel=0$, $\mathbf{k}_\parallel(\text{internal}) = \mathbf{k}_\parallel(\text{incident}) = (2mE_k/\hbar^2)^{1/2}\sin\theta$, where E_k is the kinetic energy of the incident electron and θ is the angle of incidence with respect to the surface normal. Furthermore, since the photon participating in the optical transition has negligible momentum, $\mathbf{k}_\parallel(\text{final}) = \mathbf{k}_\parallel(\text{internal})$. Therefore, we can determine both the energy (with respect to E_F) and parallel momentum of features in our angle-resolved IPE spectra.

In Figs. 4(a) and 4(b), the energies of features A,B,C,D, and A',B',C',D' are plotted as a function of $\mathbf{k}_\parallel$ along the $\bar{\Gamma}$-$\bar{X}$ and $\bar{\Gamma}$-$\bar{X}'$ directions, respectively. For comparison, the results of a tight-binding calculation of the TiO_2(110) surface electronic structure performed by Munnix and Schmeits[22] (MS) are included in the figures. This calculation assumes a surface geometry where the outermost bridging oxygen layer is omitted (cf. Fig. 2). The shaded areas are the projections of the bulk bands onto the SBZ of the (110) surface, with the lower band associated with $2t_{2g}$ states and the upper band the $3e_g$ levels. The heavy solid lines represent the predicted dispersions of true surface states, while the dashed lines are surface resonances.

Note that the dispersions of all the observed features

are, as expected, symmetric about the $\bar{\Gamma}$ point. Figure 4(a) shows that feature A lies near the top of the $2t_{2g}$ manifold, and its origin is suggested by the proximity of a predicted surface resonance in this band. On the other hand, analysis of a recent first-principles calculation of the bulk band structure[23] along the Γ-M line of the bulk BZ [which projects into the $\bar{\Gamma}$ point of the SBZ, cf. Fig. 2(c)] suggests the presence of a direct transition consistent with this feature. Since the predicted bands are only reported along high-symmetry directions of the bulk BZ, we cannot follow the theoretical dispersion of this direct transition away from the center of the SBZ. Upon surface contamination, all spectral features appear to be suppressed at approximately the same rate, making it

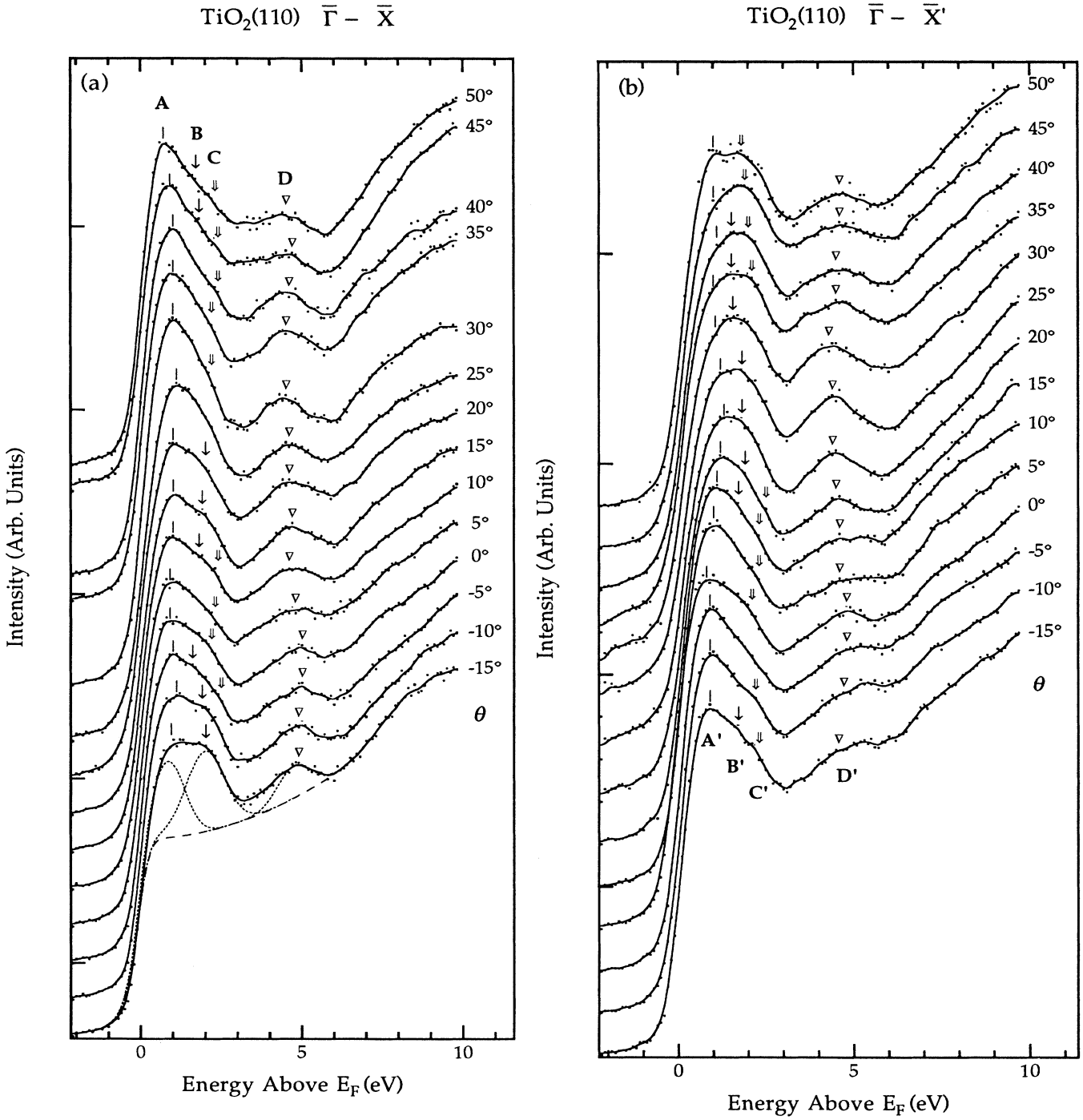

FIG. 3. Angle-resolved inverse-photoemission isochromat spectra obtained from TiO_2(110) as a function of incident electron angle with $\hbar\omega = 9.5$ eV. (a) Data obtained along the [$\bar{1}$10] ($\bar{\Gamma}$-$\bar{X}$) azimuth. (b) Data obtained along [001] ($\bar{\Gamma}$-$\bar{X}'$) azimuth.

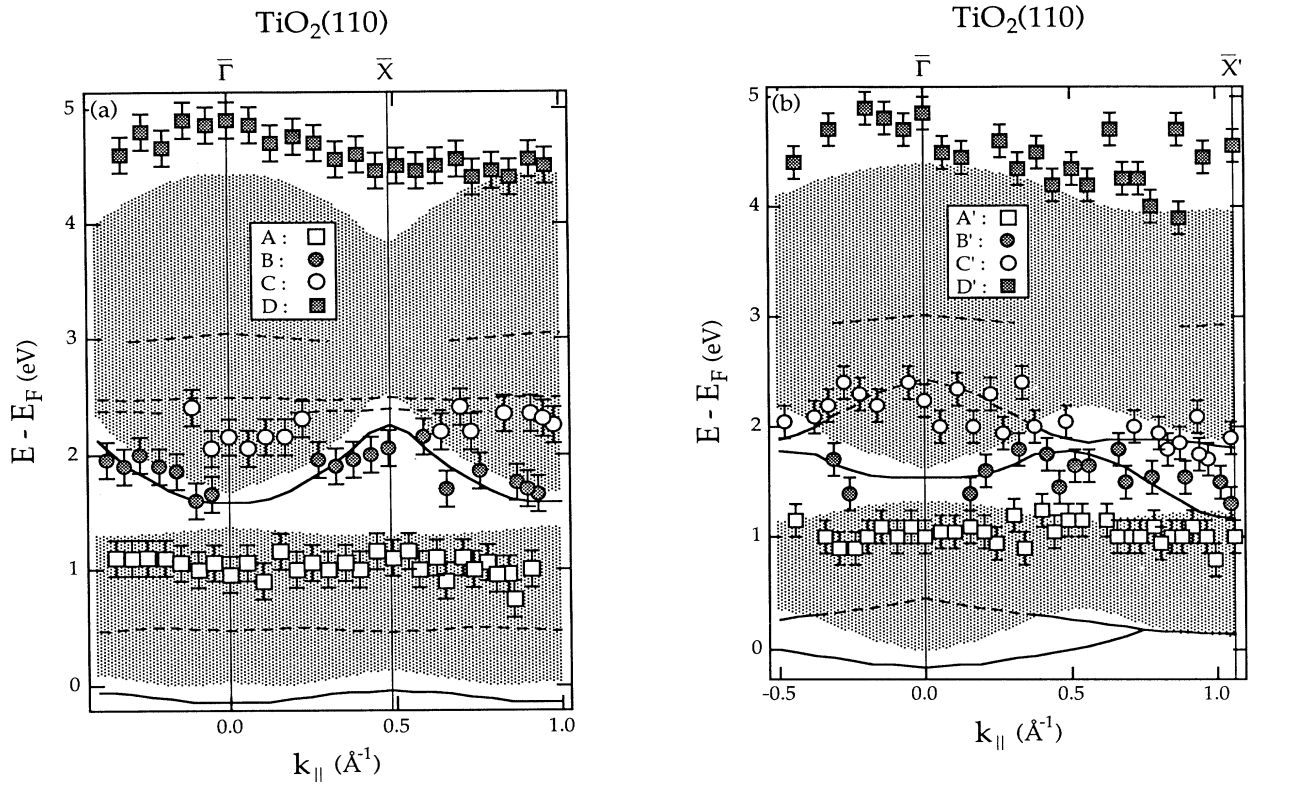

FIG. 4. Dispersion with $k_{\|}$ of the spectral features in Figs. 3(a) and 3(b). The shaded areas represent the projected bulk band on the (110) surface (Ref. 21). The heavy solid lines and the dashed lines are the predicted surface states and the surface resonances, respectively. Squares and circles are the features in Fig. 3. (a) The $\bar{\Gamma}$-$\bar{X}$ azimuth. (b) The $\bar{\Gamma}$-$\bar{X}'$ azimuth.

difficult to establish whether the experimental feature A is bulk or surface related. However, since all of the features in our spectra are consistent with predicted[22,24–26] surface states or resonances, we favor this interpretation. Experiments performed using a photon-dispersive IPE spectrograph would prove useful in better distinguishing between these two possibilities. Feature B cannot be unambiguously observed at some angles of incidence, but, when it appears, it follows the predicted surface-state dispersion quite well. Similarly, feature C lies near the series of surface resonances predicted at ~ 2.5 eV above E_F. The high-energy feature D appears to lie above the $3e_g$ band, as predicted by MS.[22] However, when the bridging O layer is included in the calculation,[22,24,25] a new surface resonance is found near the top of this band. Furthermore, calculations of the bulk band structure indicate[23,27,28] that this band extends ~ 5 eV above the conduction-band edge. On the basis of these considerations, we attribute this feature to emission from a surface resonance in the $3e_g$ band. We also note that the exact location of peak D was more dependent on surface preparation than were the low-energy features. This may be due to the fact that, while the $2t_{2g}$ levels are directed along the Ti-Ti axes, the $3e_g$ orbitals are directed along the Ti-O bonds[23,29] and are therefore expected to be more sensitive to the precise defect and vacancy concentration at the surface.

Although the scatter in the data is somewhat larger along the $\bar{\Gamma}$-$\bar{X}'$ direction, Fig. 4(b) shows a similar correlation between the predicted[22,24,25] surface electronic structure and the main features observed in the IPE spectra. Feature A' may again be attributed to either a surface resonance or a direct transition between bulk bands. Features B' and C' are consistent with predicted surface resonances near $\bar{\Gamma}$ and surface states near the SBZ boundary. It is interesting to observe that the intensity of these features begins to dominate the spectrum in the region where the calculation predicts that they are well-defined surface states near the middle of the $2t_{2g}$-$3e_g$ gap. Feature D' is, again, associated with the $3e_g$ band.

In assessing the comparison between theory and experiment summarized in Figs. 4(a) and 4(b), there are two predicted surface features that are conspicuous by their absence in the experimental data: the surface states predicted at the bottom of the conduction band, and the surface resonance near 3 eV. The absence of both of these features can be attributed to the surface geometry assumed by the electronic-structure calculation.[22,24,25] As pointed out earlier, the predicted bands shown in Fig. 4 were based on a calculation that neglected the bridging oxygen layer shown in Fig. 2. When the calculated surface density of states (DOS) is projected onto specific sites,[22] only predicted surface resonances associated with Ti(2) surface atoms have corresponding features in the

experimental data. Furthermore, the calculations[22] indicate that the Ti(2) resonances are relatively insensitive to the presence or absence of the bridging O layer. In contrast, the surface state at the conduction-band edge and the surface resonance at ~ 3 eV above E_F are primarily localized around Ti(1) atoms. When a bridging oxygen layer is included in the calculation,[22,24–26] the surface resonance and the surface state are eliminated because the coordination number of the Ti(1) ion changes from a highly undercoordinated value of 4 to a value of 6, as it would have in the bulk. We therefore believe that our observations strongly support the models of the surface geometry that include bridging oxygen rows.[1] Of course, we cannot comment on the details of atomic positions based on our results.

The presence of bridging oxygen on this surface is further supported by IPE spectra from the ion-bombarded (110) surface, on which at least a fraction of the bridging oxygen atoms is removed. Figure 5(a) shows two typical IPE spectra from a lightly ion-bombarded surface[14] (curves *b* and *c*). For comparison, a spectrum from the nearly perfect surface is also shown (curve *a*). In this figure, all of the spectra have been normalized to the same count rate at high kinetic energy. Although this normalization scheme is not unique, it is consistent with a normalization to a constant electron dose. Any other reasonable normalization scheme does not change the qualitative results of this comparison. The major change in these spectra upon ion bombardment is the appearance of increased spectral weight near 3 eV above E_F [Fig. 5(b)]. This is what might be anticipated based on the MS calculations,[22,25,26] which predicted that the surface resonances at ~ 3 eV above E_F would be created if the outermost oxygen layer was removed. A more detailed study on the defective TiO_2(110) surface is published elsewhere.[14]

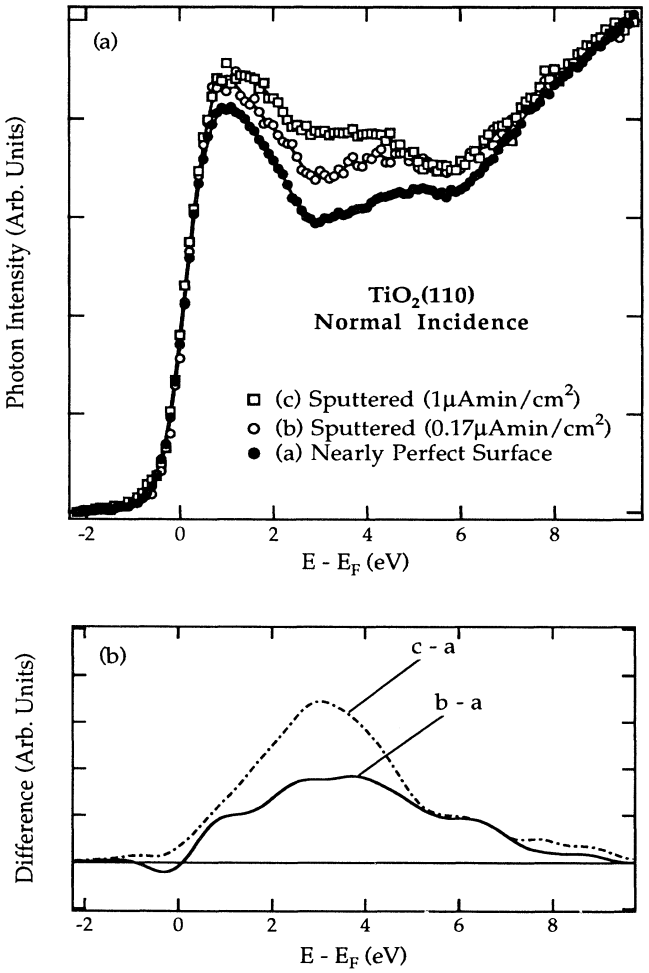

FIG. 5. (a) Inverse-photoemission spectra obtained at normal incidence from the nearly perfect and ion-bombarded TiO_2(110) surfaces. Ion doses are quoted in the legend. (b) Difference curves taken by subtracting the nearly perfect surface spectrum from the spectra of the ion-bombarded surfaces.

Although this is the first direct determination of the empty levels at a TiO_2 surface, the unoccupied electronic states of bulk TiO_2 have been investigated using a number of different spectroscopies, and these observations can be compared to our IPE results. In an early XAS study, Tsutsumi, Aita, and Ichikawa[12] observed two near-edge features at ~ 1 and 4 eV above E_F, respectively, in the Ti *K*-edge adsorption spectrum from rutile TiO_2 samples. These two features were identified as transitions to unoccupied $2t_{2g}$ and $3e_g$ orbitals, respectively, based on a MO interpretation. Transitions to these two orbitals were also observed in later EELS studies of O *K* edge and Ti $L_{2,3}$ edges, as well as in synchrotron-radiation-based XAS studies of the Ti *K* edge.[10,11] The broad emission features centered at ~ 1.5 and 4.5 eV in our inverse photoemission spectra, which we have associated with $2t_{2g}$ and $3e_g$ orbitals, are in general agreement with the two near-edge features in the Ti *K*-edge XAS data as shown in Fig. 6. However, if feature *A* is aligned with the first near-edge feature of XAS spectrum, feature *D* of our spectra occurs ~ 0.5 eV higher in energy. This slight discrepancy is consistent with feature *D* originating near the top of the $3e_g$ band.

At higher energies, large differences are seen between our IPE spectra and the XAS data. Figure 6 shows that two features are present in the IPE spectra at ~ 9 and ~ 13 eV above E_F. These are in the same general energy range as the features labeled *B* and *C* in the XAS data,[11] but occur at quite different energies. There has been considerable discussion in the literature regarding the assignment of the third and the fourth peaks above the onset in XAS spectra of the Ti *K*-edge. These two features were identified by Fischer[9] in earlier spectra as the Ti $1s \rightarrow 3a_{1g}$ and Ti $1s \rightarrow 4t_{1u}$ transitions, respectively. However, since the $3a_{1g}$ orbitals are derived primarily from Ti 4*s* levels, Tsutsumi[12] argued that the 1*s*-to-4*s* transition should be too weak to be observed due to dipole selection rules, and hence assigned *B* and *C* as $4t_{1u}$ and $5t_{1u}$ levels. It has also been suggested[10,30] that feature *B* may arise from many-body effects where a $1s \rightarrow 4p$ transition is accompanied by a "shake-down" excitation in the highest ligand orbital. On the other hand, since the same weak feature was observed in their EELS

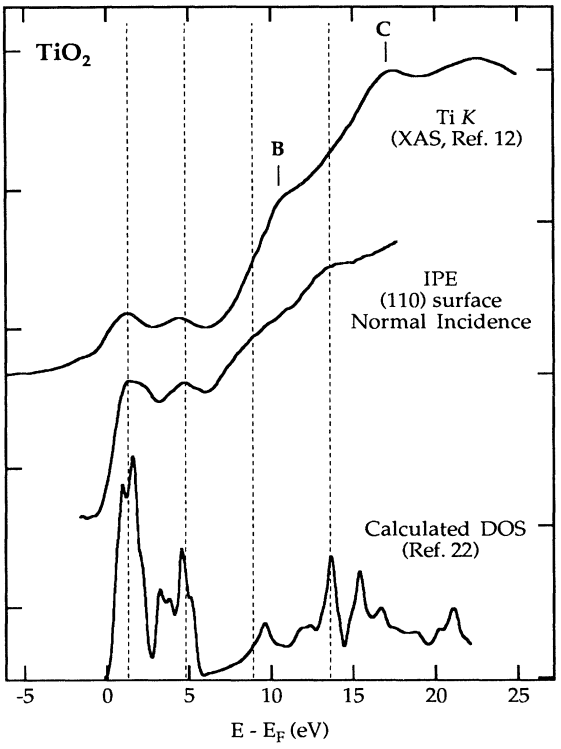

FIG. 6. The inverse-photoemission spectrum of $TiO_2(110)$ in comparison with the x-ray-absorption K edge of Ti in rutile TiO_2 (Ref. 12) and calculated DOS of rutile TiO_2 (Ref. 22). See text for details.

spectra of the O K edge, where the transition to $3a_{1g}$ is dipole allowed, Grunes *et al.*[10,11] favored Fischer's assignment.

Despite the availability of recent high-resolution XAS studies combined with more sophisticated theoretical calculations,[27,31] the situation remains unclear. Poumellec, Durham, and Guo[27] calculated the Ti K-edge absorption spectrum within the dipole approximation, using the results of a self-consistent band-structure calculation employing the local-density approximation. They found that feature C was well reproduced by their calculation, but feature B was essentially absent. Extending the calculations to include quadrupole terms did not improve agreement with experiment, and they concluded that feature B is most likely due to many-electron effects as described above. In contrast, based on a multiple-scattering calculation, Brydson *et al.*[31] obtained theoretical XAS spectra that clearly exhibit structure consistent with feature B, and interpreted this as a transition to the $4t_{1u}$ orbital.

The discrepancy between our IPE spectra and the XAS data may have several origins. First, the fact that IPE does not excite a core hole suggests that the many-body effects invoked to explain feature B in the XAS data are not expected to be important. In addition, EELS and XAS spectra tend to be dominated by dipole transitions that project out the l-dependent DOS at the site of the core hole. Calculations of the high-energy conduction bands of TiO_2 indicate[23,27,31] that the Ti $4p$ DOS becomes pronounced at a significantly higher energy than the total DOS. The comparison in Fig. 6 between our spectrum, the XAS data, and the total DOS calculated from first principles are consistent with this conclusion.

IV. SUMMARY

Angle-resolved inverse-photoemission spectroscopy has been used to study the unoccupied electronic states of the nearly perfect $TiO_2(110)$ surface along the $\bar{\Gamma}$-$\bar{X}$ and $\bar{\Gamma}$-$\bar{X}'$ directions of the SBZ. Features associated with the Ti-derived $2t_{2g}$, $3e_g$, $3a_{1g}$, and $4t_{1u}$ levels appear in our IPE spectra, and their energies agree well with theoretical predictions as well as earlier experimental results using different techniques. All of the experimental features exhibit a weak dispersion with $k_{\parallel}$, indicating that the corresponding electronic states are relatively localized, and agree well with predicted[22] surface states and resonances. Our results also provide strong evidence that the nearly perfect $TiO_2(110)$ surface is terminated by a bridging oxygen layer, as suggested by some earlier studies.[1]

ACKNOWLEDGMENTS

This research was supported by the National Science Foundation under Grant No. DMR89-07553. Valuable assistance from S. Yang and K. C. Garrison during the data-acquisition phase of this experiment is gratefully acknowledged. We also thank M. Schmeits for providing results of his calculations prior to publication.

*Present address: Department of Physics, University of Chicago, 5720 S. Ellis Ave., Chicago, IL 60637.

[1] V. E. Henrich, Rep. Prog. Phys. **48**, 1481 (1985).
[2] W. Göpel, G. Rocker, and R. Feierabend, Phys. Rev. B **28**, 3427 (1983).
[3] R. L. Kurtz, R. Stockbauer, T. E. Madey, E. Román, and J. L. D. Segovia, Surf. Sci. **218**, 178 (1989).
[4] V. E. Henrich, G. Dresselhaus, and H. J. Zeiger, Phys. Rev. Lett. **36**, 1335 (1976).
[5] Y. W. Chung, W. J. Lo, and G. A. Somorjai, Surf. Sci. **64**, 588 (1977).
[6] V. E. Henrich and R. L. Kurtz, Phys. Rev. B **23**, 6280 (1981).
[7] R. H. Tait and R. V. Kasowski, Phys. Rev. B **20**, 5178 (1979).
[8] Z. Zhang, S. Jeng, and V. E. Henrich, Phys. Rev. B **43**, 12 004 (1991).
[9] D. W. Fischer, Phys. Rev. B **5**, 4219 (1972).
[10] L. A. Grunes, R. D. Leapman, C. N. Wilker, R. Hoffmann, and A. B. Kunz, Phys. Rev. B **25**, 7157 (1982).
[11] L. A. Grunes, Phys. Rev. B **27**, 2111 (1983).
[12] K. Tsutsumi, O. Aita, and K. Ichikawa, Phys. Rev. B **15**, 4638

(1977).
[13]W. Göpel, J. A. Anderson, D. Frankel, M. Jaehnig, K. Philips, J. A. Schäfer, and G. Rocker, Surf. Sci. **139**, 333 (1984).
[14]A. K. See and R. A. Bartynski, J. Vac. Sci. Technol. A **10**, 2591 (1992).
[15]N. G. Stoffel and P. D. Johnson, Nucl. Instrum. Methods A **234**, 230 (1985).
[16]G. Denninger, V. Dose, and H. Scheidt, Appl. Phys. **81**, 375 (1979).
[17]V. Dose, T. Fauster, and R. Schneider, Appl. Phys. A **40**, 203 (1986).
[18]S. Yang, K. Garrison, and R. A. Bartynski, Phys. Rev. B **43**, 2025 (1991).
[19]S. Yang, Ph.D. thesis, Rutgers University, 1992.
[20]Commerical Crystal Laboratories Inc., 4406 Arnold Ave, Naples, FL 33942.
[21]The background generated by electron-hole pair production is expected to rise monotonically with an approximately quadratic dependence on energy for the first ~6 eV above threshold [V. Dose and G. Reusing, Appl. Phys. **23**, 131 (1980)]. In addition, for other systems where direct transitions near the Fermi level are absent, calculated and experimentally measured KRIPES spectra show a steplike onset at threshold followed by a relatively constant emission profile [see, for example, G. Borstel and G. Thörner, Surf. Sci. Rep. **8**, 1 (1987)]. The background we have chosen is an attempt to account qualitatively for both of these effects.
[22]S. Munnix and M. Schmeits, Phys. Rev. B **30**, 2202 (1984).
[23]K. M. Glassford and J. R. Chelikowsky, Phys. Rev. B **46**, 1284 (1992).
[24]S. Munnix and M. Schmeits (private communication).
[25]S. Munnix and M. Schmeits, Phys. Rev. B **28**, 7342 (1983).
[26]S. Munnix and M. Schmeits, Phys. Rev. B **31**, 3369 (1985).
[27]B. Poumellec, P. J. Durham, and G. Y. Guo, J. Phys. Condens. Matter. **3**, 8195 (1991).
[28]M. A. Khan, A. Kotani, and J. C. Parlebas, J. Phys. Condens. Matter. **3**, 1763 (1991).
[29]J. B. Goodenough, Prog. Solid State Chem. **5**, 145 (1971).
[30]R. A. Bair and W. A. Goddard, Phys. Rev. B **22**, 2767 (1980).
[31]R. Brydson, H. Sauer, W. Engel, J. M. Thomas, E. Zeitler, N. Kosugi, and H. Kuroda, J. Phys. Condens. Matter. **1**, 797 (1989).